Experimental investigation on the dynamic response of RC flat slabs after a sudden column loss

J.M. Russell[a,*], J.S Owen[a], I. Hajirasouliha[b]

[a] *Faculty of Engineering, The University of Nottingham, UK*
[b] *Department of Civil and Structural Engineering, The University of Sheffield, UK*

Abstract

To prevent disproportionate collapse under an extreme loading event, a sudden column loss scenario is often used to ensure the structure has suitable robustness. This study aims to investigate experimentally the dynamic response of reinforced concrete flat slabs after a sudden column loss. Seven 1/3 scale reinforced concrete flat slabs were tested under static load increases or dynamic column removal cases with different supports removed. Reaction forces and deflections were recorded throughout, along with reinforcement strains and concrete cracking patterns. During dynamic tests, a high speed camera was used to capture the dynamic motion. The experiments demonstrated that flat slabs, in general, are able to redistribute their loading effectively after a column loss. Although large levels of damage were observed, collapse due to flexural failure did not occur. However, punching shear was shown to be an issue due to the additional vertical loading on the adjacent supports. The inclusion of continuous bottom reinforcement through a column did not significantly improve the capacity, as the new load path is not primarily through the removed column location. The results also indicate that the dynamic effects due to a sudden column loss can be significant as deflections of up to 1.5 times the static case were measured within the elastic range. It is also shown that

*Corresponding author.
Email address: evxjr@nottingham.ac.uk (J.M. Russell)

the Dynamic Amplification Factor (DAF) reduces when nonlinear damaging effects are included, which implies conventional code-based design methods for flat slab structures may be over conservative. Additionally, the increase in material strength due the strain rates is not viewed to be significant.

Keywords: Progressive Collapse, Column Loss, RC Flat Slab, Punching Shear, Dynamic Amplification

1. Introduction

The issue of protecting structures against progressive failure has been a key part of design considerations since the collapse of Ronan Point tower block in 1968, where a relatively small gas explosion on the 18th floor led to the collapse of a corner of the structure resulting in several deaths [1]. The issue arose again after the bombing of a federal building in Oklahoma, involving a car bomb damaging an external column that was supporting a transfer beam. The partial collapse killed 168 people, the majority due to the collapse progressing through the structure, rather than in the direct blast area [2, 3]. Progressive failure, mainly due to punching shear, has also occurred on flat slab structures, including the Pipers Row car park (1997) [4] and Sampoon Department store (1995) [5]. As a result of these events, design codes usually require consideration of the potential for progressive collapse. This is commonly achieved by ensuring that the structure can survive the accidental removal of an individual member without experiencing disproportionate damage [6].

This situation has been investigated by a number of authors to determine the failure mechanisms and ultimate capacity of Reinforced Concrete (RC) frames after a column loss event. These have included experimental tests on Reinforced

Concrete (RC) frames [7–9]. Sasani et al. has conducted a number of tests on real structures to investigate the global response and potential for progressive failure of RC structures [10–13]. The importance of nonlinear effects, both material and geometric, has been highlighted in providing additional capacity and preventing progressive failures. However, sufficient ductility is required to allow yielding and the development of catenary action, otherwise brittle failures may occur.

Further consideration has been given to the presence of slab elements, which have been shown to increase the capacity of a structure after a column loss [14, 15]. RC slabs have complicated behaviour at high deflections due to their two dimensional nature allowing formation of tensile and compressive membranes [16–19]. Furthermore, their susceptibility to brittle mechanisms such as punching shear [20–23] may potentially lead to progressive collapse.

The general behaviour of reinforced concrete slab elements is well known, however, there has been only limited investigations into their performance against progressive collapse. Hawkins and Mitchell [24], Mitchell and Cook [25] and Yagob et al. [26] have addressed some of the issues and Yi et al. [27] recently conducted limited tests to study the quasi-static response. Their results provide valuable insights into the nonlinear behaviour but further tests are still required.

Progressive collapse is also a dynamic issue and suitable account needs to be taken of the inertial effects involved after a sudden damaging event [28, 29]. This can be done by conducting a full dynamic analysis of the structure; however this is time consuming and requires detailed information in order to achieve accurate results. Alternatively, an equivalent static case can be considered with a Dynamic Amplification Factor (DAF) applied to the loading. Current design recommendations usually suggest a DAF of 2.0 [30]. The suitability of this value has been studied for some structural types, with some authors suggesting it is over conservative [31–34]. However, further investigation is needed for flat slab structures.

This study aims to provide much needed experimental evidence for the behaviour of flat slabs after a sudden column loss, especially considering the nonlinear and dynamic effects. Scaled slab models were investigated to simulate the dynamic response of flat slab elements in different column loss scenarios. Dynamic results under different levels of loading were compared to static tests to assess the additional damage sustained due to inertial effects. Although it is recognised that the simplifications involved in the experimental programme do not completely replicate real structures, the set up is better suited for future modelling with finite element software. Additionally, the key aspects involved can still be considered, allowing future work to focus on the important factors. In particular the details regarding the redistribution of forces and the damage patterns after an extreme event provide an indication of the potential for collapse of a structure. The results from this work will later be used to validate further numerical investigations into this issue.

2. Experimental Procedure

To investigate the behaviour of in-situ RC flat slab structures, seven 1/3 scale simplified substructures were constructed, as shown in Figure 1. These allowed simulation of the removal of a corner, penultimate edge or an internal edge column. Additionally, different reinforcement layouts were considered. Two types of tests were conducted, an increase in static loading and a sudden dynamic column removal. Under the static case, the slab was placed on the supports and the column position under investigation was removed. A uniform load was then imposed across the entire sample by means of sand and gravel bags. Support reactions, deflections, strains and cracking patterns were recorded throughout. Under the dynamic removal, a similarly designed slab cast at the same time as the static, was loaded whilst fully supported. Once the required UDL was achieved, the chosen support was removed and the system allowed to deform and either reach a new equilibrium or experience total failure. During the test the response was recorded with load cells, strain gauges, LVDTs and a high speed camera.

3. Test setup

3.1. Comparison to real structures

The substructures constructed were based on a typical structural arrangement but with simplifications which made it easier to conduct the experiments and to compare the results to numerical models. Rather than replicate the partial rotational and translational restraint that slab-column connections provide, simplified supports were used. Although it is known that this does not represent conditions found in real structures, these assumptions are easier to model for later numerical analysis in order to validate material and mechanical behaviours. Additionally, under a penultimate edge column removal condition, the immediate section of slab is laterally unrestrained, as described by Dat and Hai [18], and therefore the use of such supports is not considered to affect significantly the ability of the slab to form mechanisms such as compressive rings for membrane action.

The scaled models were designed to have an equivalent demand to capacity ratio as a full size prototype based on the method presented by Kai and Li [32]. For third scale tests, span and depth values were reduced by factor of 3, UDL by 1 and reinforcement areas by 3 and therefore the reinforcement ratios were kept constant. The span to depth ratio of all the specimens was 25, which is within the range of values for typical flat slab structures.

3.2. Slab design

All the slabs were designed to Eurocode 2 [35]. Along with the slab self-weight, the design considered additional finishes of $1kN/m^2$ and a variable action of $2.5kN/m^2$. The characteristic cube strength used in the design was 30MPa. Details of the test specimens are given in Table 1 along with concrete cube strengths taken from samples on the day of testing. Some variation in the concrete strength can be seen between the tests, and the concrete is below its target strength for tests C-S and C-D. However, for the majority of the discussion, comparisons are only made between tests with similar strengths.

For the first six tests, a 2x1 bay subsection of a flat slab structure was constructed. The specimens were 4100mm x 2100mm in plan with a thickness of 80mm. Each sample included two A142 meshes providing 6mm bars at 200mm spacing for both top and bottom reinforcement (ρ = 0.18%). Additional 6mm bars were added over internal supports in the column strip to meet requirements for the hogging moment (ρ = 0.21%). No shear reinforcement was included as the concrete alone provided enough capacity for a fully supported condition according to Eurocode requirements. This set up was used to replicate both the corner (C) and the penultimate (P) column loss as shown in Figure 1(a). The reinforcement design provided the minimum reinforcement area for both top and bottom steel according to Eurocode 2 [35], a condition that governed in the middle strips. For comparison purposes an equivalent series of tests were conducted without bottom rebar through the column location for the penultimate location tests, designated PC and PR, where C indicates continuous and R indicates reduced.

The final test considered a middle (M) column removal using a 4x1 bay system, constructed in the same manner, with a total length of 8100mm (Figure 1(b)).

3.3. Support details

The supports were 135mm square steel plates, 25mm thick, on hemispherical bearings to allow rotations. The supports were considered to be pinned, free to rotate in any direction and allow the slab to uplift, see Figure 1(c). For the dynamic tests, a temporary support that could be quickly removed was constructed. The temporary support was designed based on a vertical steel bar between two steel plates. The bottom plate rested on a load cell and steel rollers to allow the support to move easily. The removal process used is shown in Figure 2. During the pre-loading period, chocks were placed to prevent lateral movement and a clamp placed around the bar to ensure it remained upright; see Figure 2(a) for details. Once the required loading was reached, and the laboratory area around the test had been cleared, the temporary supports and clamps were removed to create an unstable condition (Figure 2(b)). Finally, a rope attached to the bar was pulled sharply, causing the support base to move and the bar to disengage with the slab, as in Figure 2(c). This system did not cause a true instantaneous removal, however, as the purpose of these tests is to provide information to validate a numerical model, this limitation will be addressed in later work.

An example of the test set up is given in Figure 3 showing a fully loaded sample prior to the sudden removal of the front middle support.

3.4. Instrumentation

Each support included a load cell to measure the vertical reactions, see Figure 1(c). The calibration was checked before each test, with a typical uncertainty of

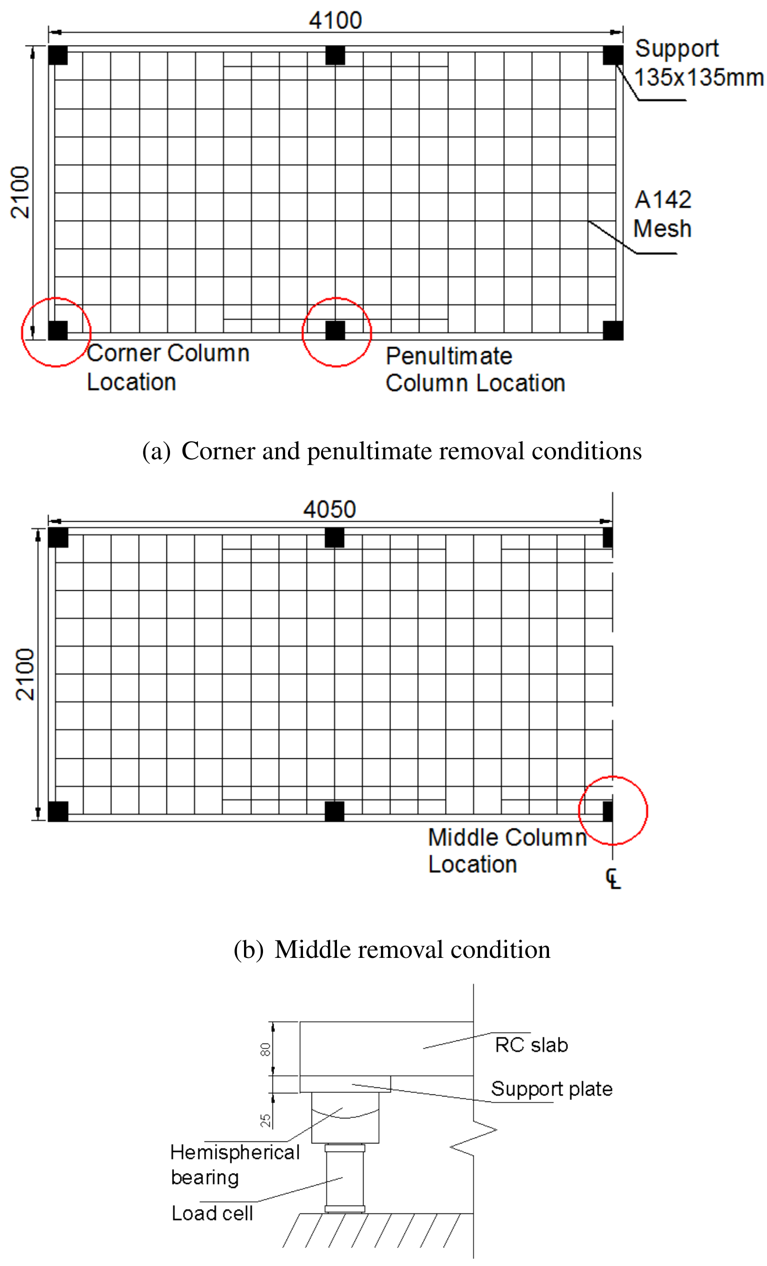

(a) Corner and penultimate removal conditions

(b) Middle removal condition

(c) Support details

Figure 1: Details of specimens

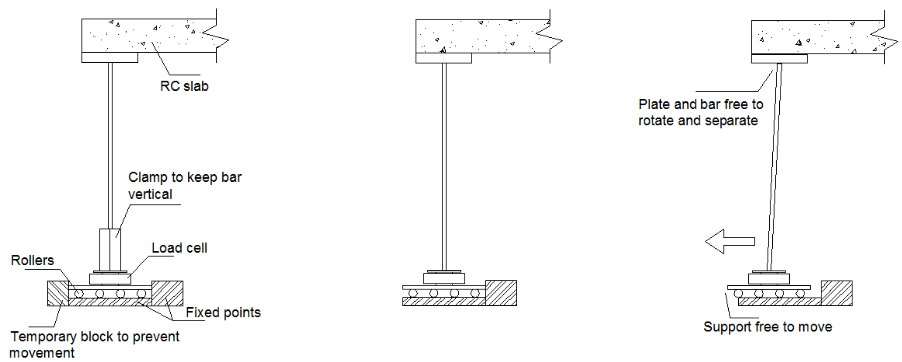

(a) Fully supported (b) Unstable condition (c) Support being removed

Figure 2: Diagram showing the process of removing the temporary support for dynamic tests

Table 1: Test details and IDs

Slab ID	Removal Position	Reinforcement	Test Type	Cube Strength (MPa)
C-S	Corner		Static	24.4
C-D	Corner		Dynamic	26.7
PC-S	Penultimate	Continuous	Static	33.9
PC-D	Penultimate	Continuous	Dynamic	37.1
PR-S	Penultimate	Reduced	Static	33.8
PR-D	Penultimate	Reduced	Dynamic	35.2
M-D	Middle		Dynamic	30.6

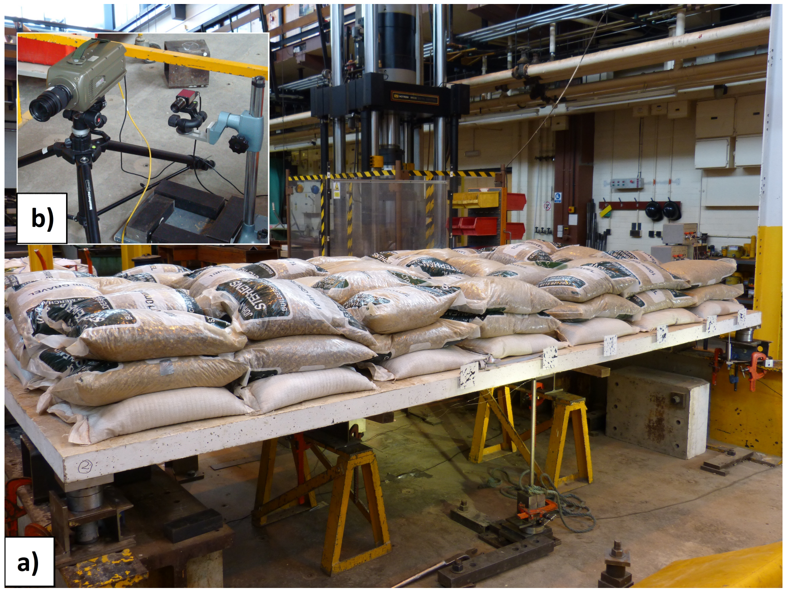

Figure 3: a) Photograph of slab PC-D before dynamic testing; b) Cameras for visual monitoring

50N per load cell, leading to total uncertainties of 0.25, 0.30, 0.45 and 0.5kN for configurations using 5, 6, 9 and 10 load cells respectively. Measuring support reactions before column removal allowed the slab to be balanced correctly. Once a column had been removed, the changes in reactions at the remaining supports allowed the redistribution of forces to be determined. Measurements taken during the tests showed changes in demand to each support as the specimen experienced damage.

An array of Linear Variable Displacement Transducers (LVDTs), sampled at 250Hz, were placed under each specimen to measure vertical deflections. Around the column loss location, Digital Image Correlation (DIC) techniques were also used to monitor deformations. Camera footage combined with video gauge software [36] measured the static deflections at points across the sample. The positions of the presented measurement points for tests C, PC and PR are given in Figure 4. For the dynamic tests, a Phantom v12.1 high speed camera was utilised to capture the behaviour in the short time period during and after the column removal (see Figure 3(b)). Images were recorded at 2500fps with an exposure of 300μs and then processed by the video gauge software to obtain deflection readings and to estimate the column removal time. Based on the size of the visual targets, distance of the camera and processing software used, an accuracy of $\pm 0.1mm$ was achieved. The high speed footage was also used to identify crack propagation patterns. Throughout each test, strain gauges were used to determine the stress distributions with the aim of providing information on the critical areas and potential for failure. The locations of the strain gauges on the reinforcing steel that gave usable data are also shown in Figure 4.

4. Experimental Results

For the dynamic removal tests, the high speed footage was analysed to estimate the time taken for the support to be removed. This was based on the period between the rope attached to the support becoming taught with the bar starting to move and the moment that either the bar was clearly disengaged with the support plate, or the plate was no longer in contact with the slab. This method is likely to overestimate the removal time, as it does not take account of the condition where the support plate and slab remain in contact, moving vertically at the same rate whilst not transferring forces. A summary of removal times for each test is given in Table 2.

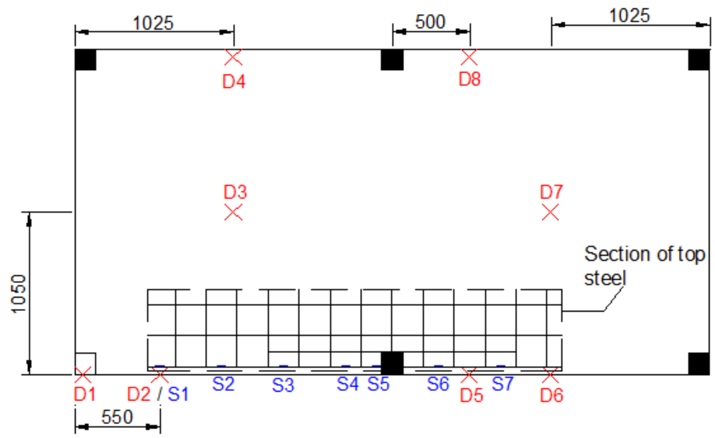

(a) Corner condition

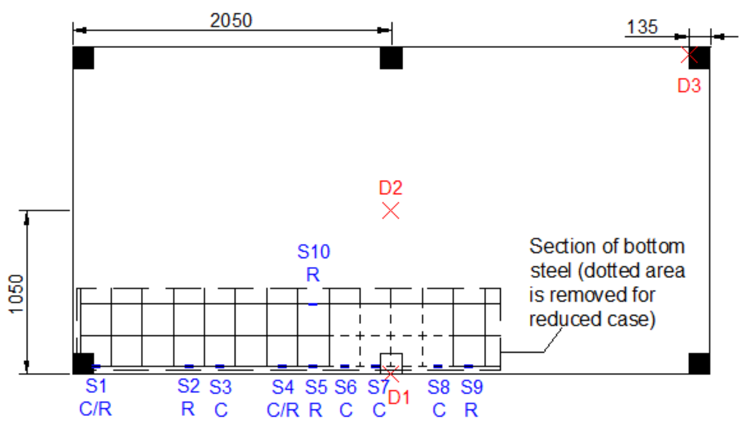

(b) Penultimate removal conditions - Continuous (C) and Reduced (R)

Figure 4: Locations of LVDTs and visual targets (D) and strain gauges (S)

Table 2: Estimated column removal times for each test

Slab ID	Loading Level (kN/m^2)	Estimated time (ms)
C-D	3.0	53.2
	6.8	57.0
	7.7	50
PC-D	2.5	40
	5.6	50
PR-D	2.3	52.5
	5.7	39
M-D	3.1	33.7
	6.7	49.2
	8.5	42.6
Average		46.7

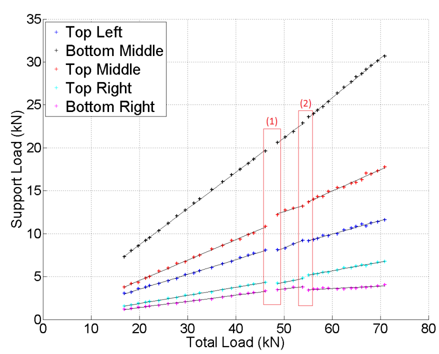

(a) Vertical reaction to each support

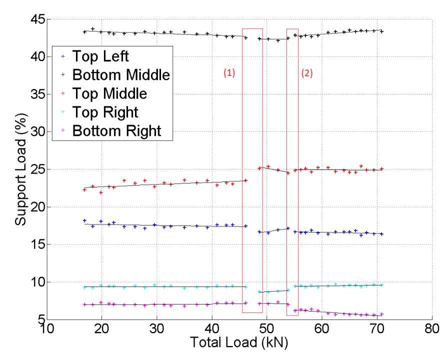

(b) Percent of total load to each support

Figure 5: Distribution of forces to supports - Test C-S

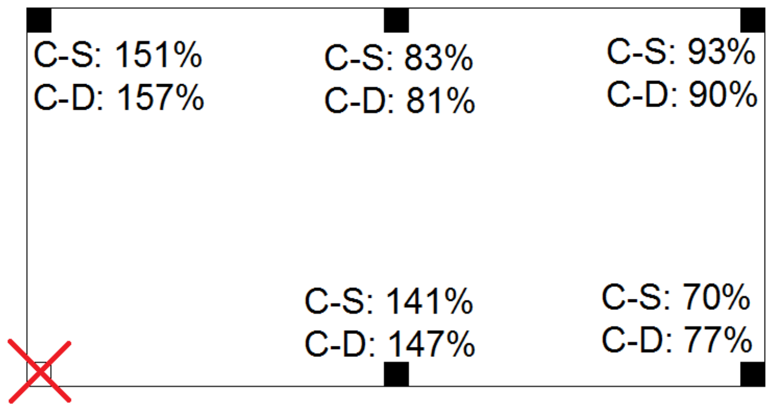

Figure 6: Mean change in distribution of forces to each support after corner column loss - Tests C-S and C-D

4.1. *Corner position*

4.1.1. *Static loading test*

Figure 5(a) shows the vertical reactions at the supports during the corner static test (C-S) (see Table 1). As it was expected, the reaction forces increased linearly by increasing the total load in the elastic range. However, beyond 46.2kN total load (5.4kN/m^2) there was a change in distribution (label 1) until approximately 55kN (6.4kN/m^2), coinciding with the formation of cracking across the element. Past this phase (label 2) there is a linear increase of reactions again, though with a larger deviation from the trend line. The relative distribution of forces to each support given in Figure 5(b), suggests that the relative demand stayed constant in the elastic and final ranges. Between labels 1 and 2 there was again a noticeable change as redistribution of forces occurred due to extensive crack formation. Considering, however, the entire range, suggests that a linear model could be used to describe the relationship.

Comparison between the averaged reaction forces for fully supported and damaged conditions (see Figure 6) indicates that the two orthogonally adjacent supports experienced a 41-57% increase in their vertical reaction while all other supports had a decrease in demand. It should be noted that C-S and C-D showed similar ratios, indicating dynamic removal did not change the final distribution of reaction forces.

At higher levels of loading, significant flexural cracks formed due to the large increase in hogging moments in both tests, initially on the top surface over the adjacent support (Figure 7(a)). Sagging flexural cracks also formed on the underside as the slab now spanned diagonally between the two supports nearest the removal location (Figure 7(b)). The location of permanent supports (solid boxes) and the removed support (outline) are annotated in this figure.

The plot of normalised displacements, deflection (δ) / slab thickness (t), against load in the damaged bay area (Figure 8(a)) shows an initial linear response. However, after a load of 4.6kN/m^2 flexural cracks start to form resulting in a decrease in stiffness to around 57% of the initial value. At 6.0kN/m^2, when the peak displacement equals 0.19 times the slab depth, there is a discontinuity due to significant cracking over the adjacent support along with yielding of the reinforcement. This led to an increase in displacements across the entire sample, with the maximum exceeding half the slab depth. After this, there was a brief stiffening phase before a final softening with a relative stiffness of 6% of the elastic range. The slab continued to carry additional load until the test was aborted at 8.2kN/m^2. In the adjacent bay, shown in Figure 8(b), once damage occurred there was a jump in response observed in the middle (point D7, Figure 4(a)) due to the flexural sagging cracks in that area. The high deflections in the damaged area also led to a relative

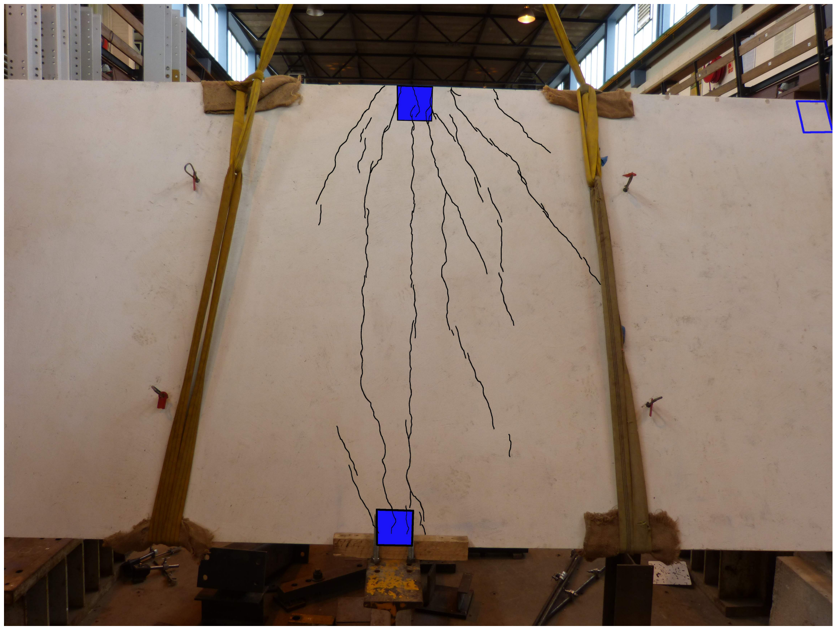

(a) Top surface

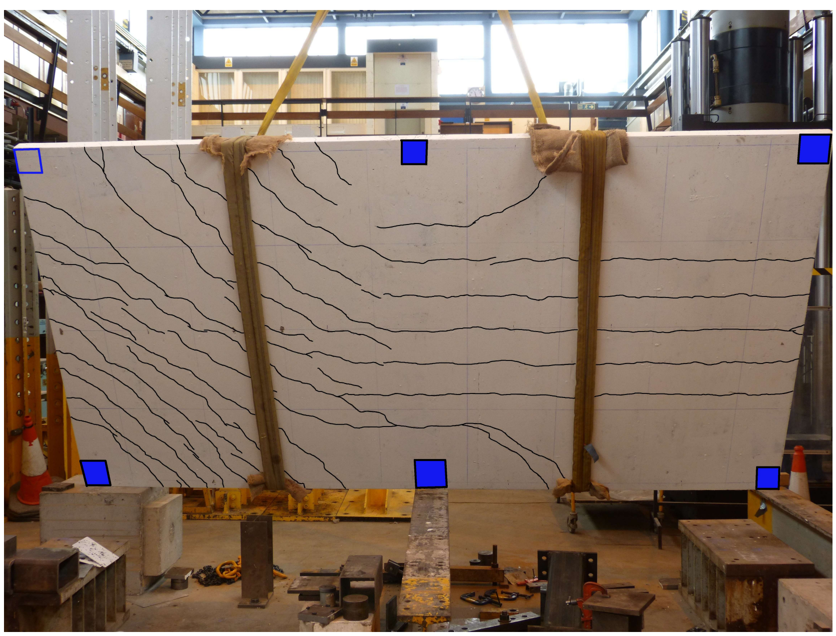

(b) Bottom surface

Figure 7: Annotated flexural cracks after corner column loss

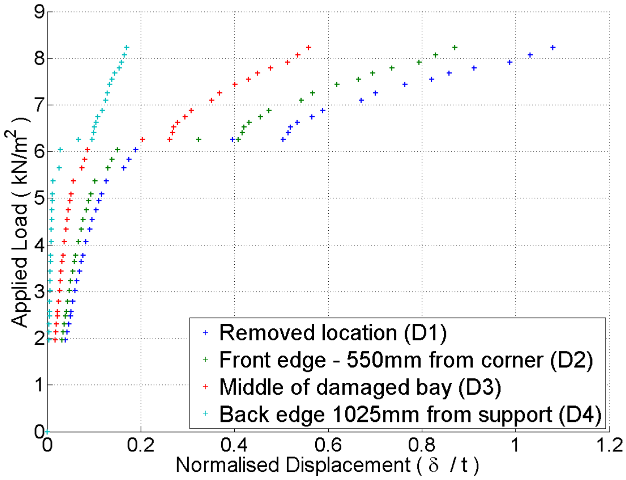

(a) Displacements in the damaged bay

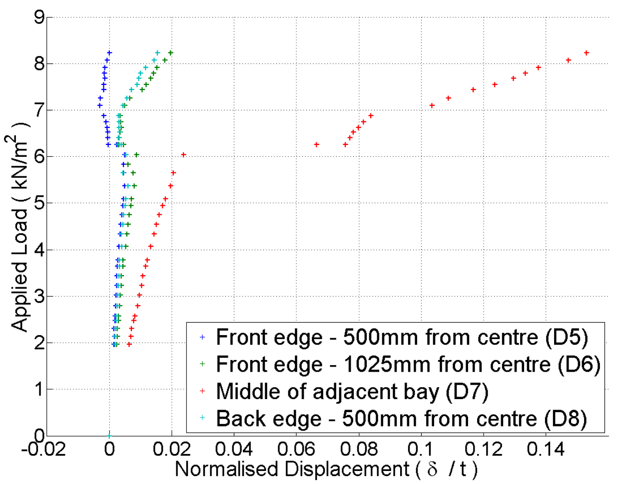

(b) Displacements in the adjacent bay

Figure 8: Load against normalised displacements - Test C-S

uplift due to the large rotation around the central support (point D5). The discontinuous response corresponds to the changes in reaction forces seen in Figure 5, as discussed in the previously.

The strain data in Figure 9 provides a further understanding of the damage profile. Strain readings have been corrected against the fully loaded condition under the slab's own self weight, i.e. the results demonstrate the change from the starting condition, and then normalised against the yield strain. Below a load of 4.1kN/m^2, strains on the steel over the central column were relatively low. However, after the formation of flexural cracking there was a peak in strain on the damaged side of the support at 6.04kN/m^2, corresponding to the large increase in displacements seen in Figure 8(a). As loading increased there was local yielding of the reinforcement in this area, while other areas remain well below the yield strain.

4.1.2. Dynamic removal test

The normalised displacements (displacement/ slab thickness) for dynamic removal at three different levels of loading are plotted in Figure 10 for the removal location and the middle of the adjacent bay (Points D1 and D7 in Figure 4(a)). Peak displacements, damped natural frequency and damping ratio results for these tests are compared in Table 3.

At 3.0kN/m^2 the structure was within the elastic range resulting in small deflections (7% and 5% of slab depth for peak and final displacements respectively). The low total mass resulted in a high frequency response, and as no damage occurred there was little dissipation of the energy. The low damping ratio ($\zeta = 0.01$) caused the system to take several seconds to return to its static equilibrium position.

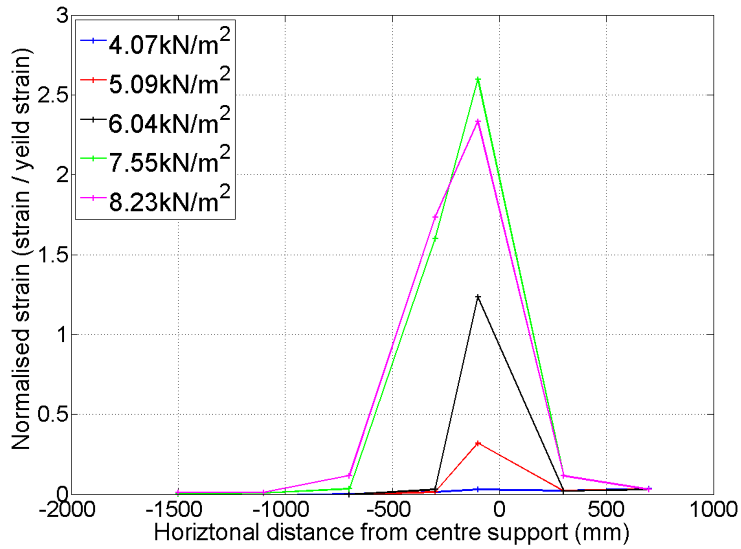

Figure 9: Normalised strain against position for top reinforcement bars - Test C-S

The specimen was then reset to the starting position and the static load increased to 6.8kN/m^2, just within the plastic region from the earlier static condition. Much higher deflections, peaking at almost 60% of the slab depth, were measured. Thin hogging cracks were observed, which resulted in a higher energy dissipation and a larger damping ratio (ζ = 0.24), however overall damage was not extensive.

For the final case the load was increased to 7.7kN/m^2 and the test repeated. Figure 11 shows the power density spectrum from a Fourier transform of displacement readings following a corner column loss at different load levels. The results indicate that for the slab in the plastic region (i.e. 7.7kN/m^2), the large deflections and resulting damage created a different response to the single dominant frequency peaks seen before. As cracks had already formed during the 6.8kN/m^2

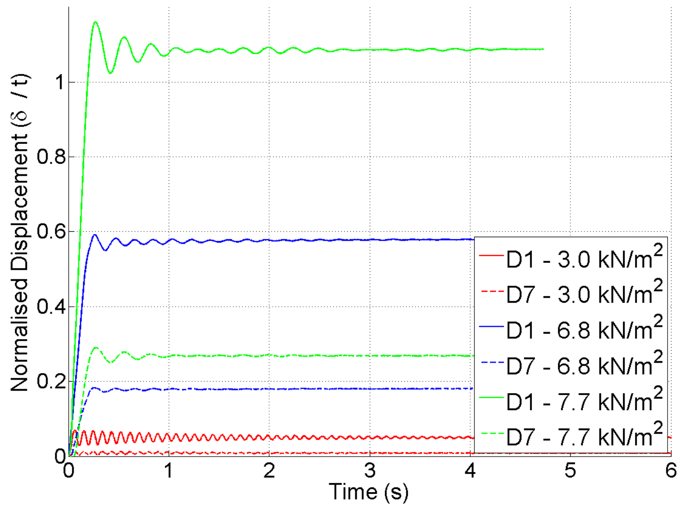

Figure 10: Normalised displacement against time after column removal at different positions and loading - Test C-D

test and subsequently widened in the next case, the friction at the crack face was reduced resulting in the smaller damping ratio observed at 7.7kN/m^2 (Table 3). Additionally, the pre-existing damage may have been a factor for the two frequency response seen. At this loading, peak deflections exceeded 110% of the slab depth but did not lead to complete failure.

Within the elastic range, the amplitude between the first peak and first dip is 60.7% of the maximum displacement, indicating the structure returns relatively close to its initial state. Once permanent damage had occurred both these ratios drop considerably as seen in Table 3.

The strain data collected during a dynamic removal also allowed estimation of the strain rates, $\dot{\varepsilon}(t)$. The tensile strain rates against time for the top steel are presented in Figure 12 for the three loading levels. Each line shows the maximum

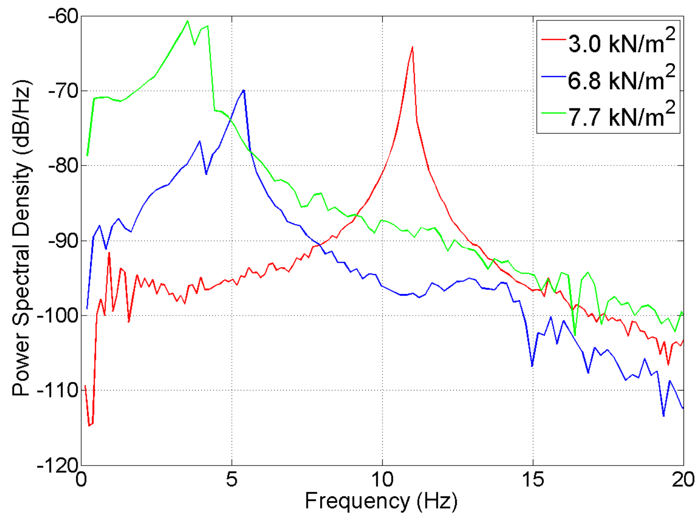

Figure 11: Power spectral density of displacement following corner column loss at different load levels - Test C-D

Table 3: Results from dynamic removal - Test C-D

Loading (kN/m^2)	3.0	6.8	7.7
Normalised Peak	0.07	0.59	1.16
Amplitude / Peak (%)	60.7	7.36	11.91
Peak / Final Displacement	1.42	1.02	1.07
Damped Natural Frequency (Hz)	11.0	5.41	3.54/4.21
Damping Ratio	0.01	0.24	0.123

strain rate that occurred at any monitored position, at each time step.

Strain gauge S5, positioned next to the central support, see Figure 4(a), experienced a much higher strain rate for each loading level. Since the graph only presents the maximum value, the response of the other gauges is hidden. Therefore, a second line is plotted excluding this sensor. Additionally, the key strain data with time, adjusted against the strain readings at the fully support condition, is also plotted on the second vertical axis to allow further comparisons.

In Figure 12(a), the elastic case, most the sensors on the top steel show very low levels of strain rates, with only sensor S5 showing a strong peak. However, it is clear that the peak strain occurs a period of time after the peak strain rate. This is significant in considering the influence of strain rate effects in increasing the material tensile capacity during sudden column losses. At 6.8kN/m^2 of loading, shown in Figure 12(b), a similar pattern is seen, however there is still a reasonable peak at other locations. Overall, high strain rates are observed here with a maximum rate of 0.153s^{-1} occurring just before the maximum strain. The change in maximum strain from the fully supported case suggests that the steel has yielded in this area; this may explain the localised high strain rate and also affect the final results.

The final loading case presented in Figure 12(c) shows a different response. The largest strain rate does again comes from sensor S5 (next to the central support), the rates and change in strains are smaller than the previous case. This is most likely due to the plastic deformations that occurred. Of further interest is sensor S3, see Figure 4(a) for its location. As this position was previously closer to the middle of the span, it was under a compressive condition and then changed to a tensile state due to the column loss. This change demonstrated itself by a

Table 4: Details of shear failures

Slab ID	Max loading (kN/m^2)	Max displacement (δ/ t)	Shear failure	Loading type at failure	Initial location	Further failure
C-S	8.2	1.08	No			
C-D	>7.7	1.54	Yes	Static push down[a]	Back left corner	Bottom middle
PC-S	6.4	2.23	No			
PC-D	6.8	1.71	Yes	Static[b]	Front left corner	
PR-S	6.7	1.67	Yes	Static	Front left corner	Front right corner
PR-D	5.7	2.12	Yes	Dynamic	Front right corner	Front left corner
M-D	9.2	0.74	No			

[a]After the final dynamic test a large load was applied over the removed corner to cause complete failure.

[b]After the final dynamic test, loading changed to a static UDL.

delay in response before the large tensile deformations occurred leading to large permanent strains. The peak rates were 0.031 and 0.034s^{-1}.

Finally the sample was loaded to failure, which occurred due to punching shear at the two adjacent supports as shown in Figure 13. Table 4 gives the shear failure details of all the slabs tested.

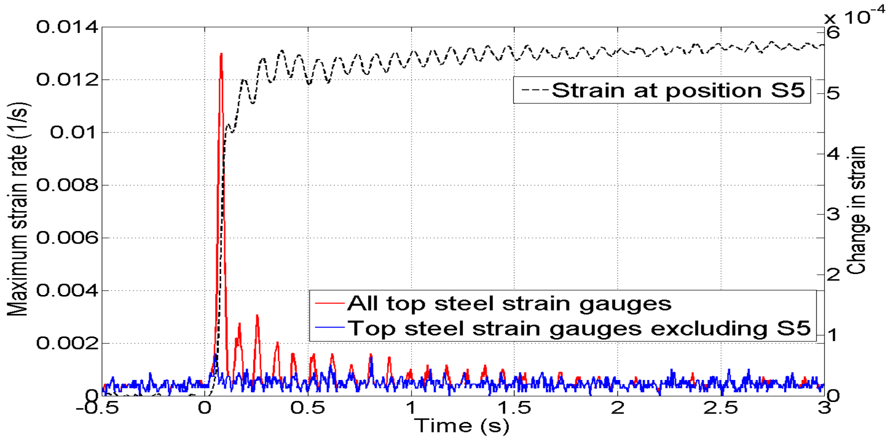

(a) 3.0 kN/m^2 loading

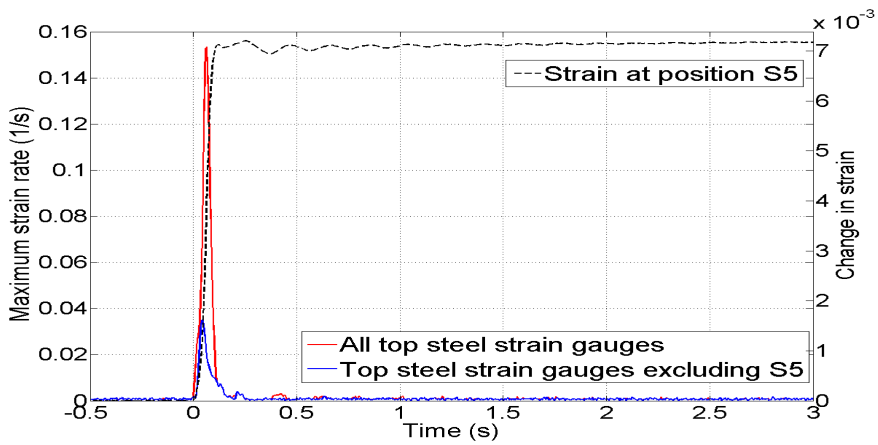

(b) 6.8 kN/m^2 loading

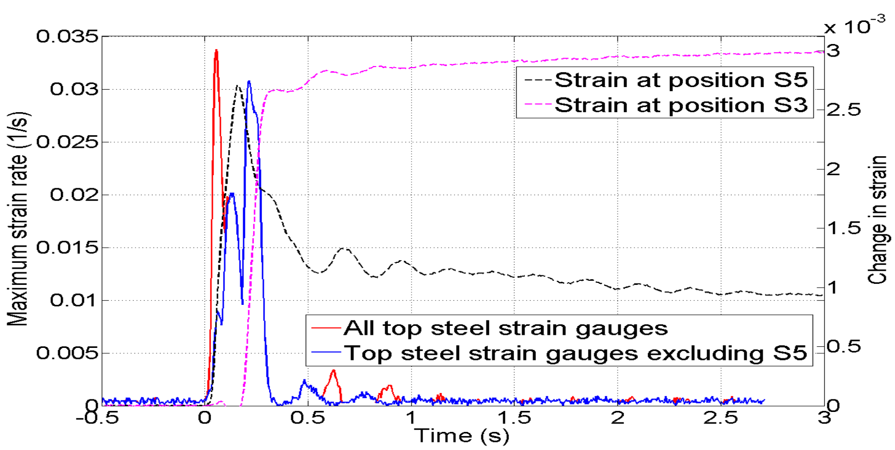

(c) 7.7 kN/m^2 loading

Figure 12: Maximum steel strain rates against time. Also showing changes in strain against time. Test C-D

Figure 13: Final state of corner removal case after shear failure - Test C-D

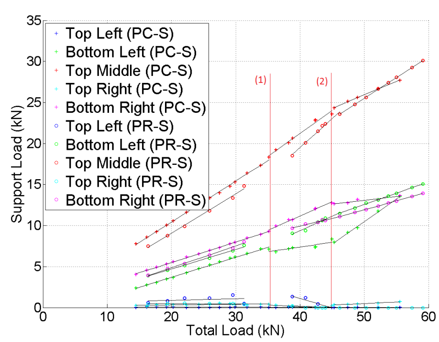

(a) Vertical reaction to each support - Tests PC-S and PR-S

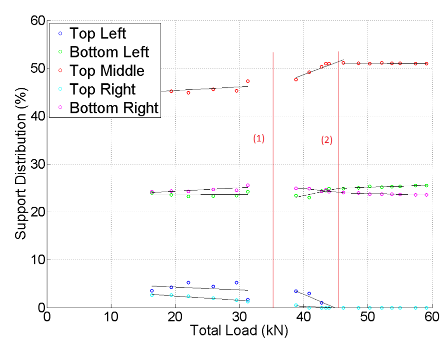

(b) Percent of total load to each support - Test PR-S

Figure 14: Distribution of forces to supports - Tests PC-S and PR-S

4.2. Penultimate position

4.2.1. Static loading test

The load increase to each support for two Penultimate removal cases with static loading are shown in Figure 14(a). Similar responses are observed for the two conditions with nearly all points showing a simple linear relationship at low loading at equivalent rates. The back middle support takes the highest proportion of loading, followed by the front corners.

Flexural cracking occurred at 35kN and 30kN of total load, for PC-S and PR-S respectively, which was followed by a period of redistribution of reaction forces across the samples until approximately 45kN, between labels (1) and (2). After this stage the distribution remains reasonably constant until failure.

The change in support reaction distribution occurred principally due to uplift at the back two corners, as a result of the large downward deflection in the middle. What little load those supports had been carrying was then taken by the other supports (Figure 14(b)), primarily the back middle.

The bottom left location in PC-S shows a more dramatic change. This was due to the load cell rotating at higher deflections, an issue that was corrected for in other tests by stabilising the load cell horizontally, and does not indicate a change in loading on the support.

Deflections of PC-S and PR-S are given in Figure 15 for the positions identified in Figure 4(b). It is shown that there is a clear linear response across all parts of the slab before cracking occurs. Additionally, the initial stiffness of the two reinforcement cases was identical. Both cases started to crack at similar points, with a slight reduction in stiffness observed after 3.4kN/m^2. This corresponds to a peak normalised displacements of 0.1. However, after peak displacement of 0.13 times

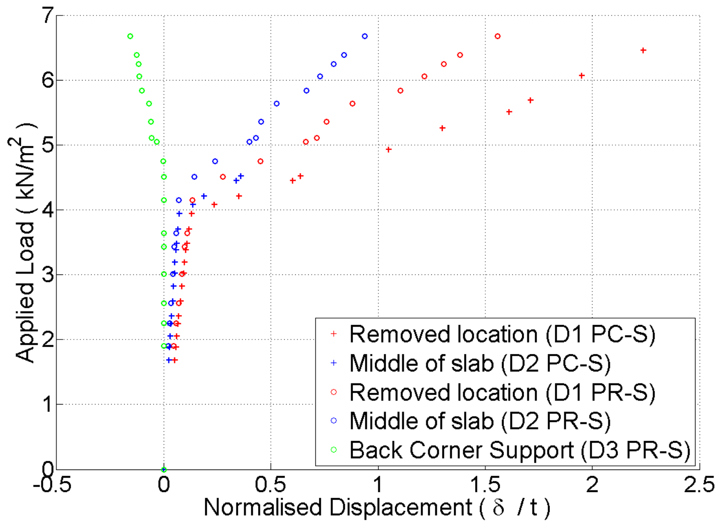

Figure 15: Load against normalised displacement for PC-S and PR-S

the depth there is a significant reduction in stiffness due to more extensive flexural cracking. After this point there was a linear trend for the remaining data, though the new stiffnesses were less than 5% of the initial values. In the corner removal case there was a large increase in displacements as cracking formed, which does not occur here. The geometry of these tests meant that sagging cracks were the most significant form of damage and these were spread out across the midspans and so did not cause the sudden drop in stiffness observed from the very localised hogging cracks in the previous test. The results also demonstrate the uplift effect experienced at the back support (point D3 in Figure 4(b)), as shown by the negative displacement.

The reduced case experienced a sudden shear crack of the front left support at 6.7kN/m^2 with an approximate shear force of 15.1kN. The corner sections had a designed shear capacity of 12.6kN according to Eurocode 2. As soon as this

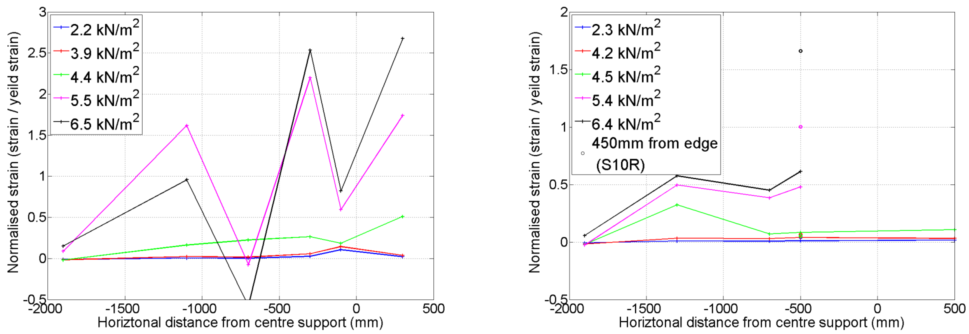

(a) Continuous reinforcement - Test PC-S (b) Reduced reinforcement - Test PR-S

Figure 16: Normalised strain against position for bottom reinforcement bars

failure occurred, the second front corner support also failed by shear (see Table 4). Test PC-S was ended due to safety concerns at a lower loading than the level that caused shear failure in PR-S, although the design shear capacity had already been exceed. Had the test been continued it is likely that a similar failure would occur. The rotation of the load cells, and therefore support conditions, for the continuous reinforcement test also resulted in the higher deflected profile without causing shear failure.

Figure 16 shows the strain profiles of the bottom reinforcement bars for tests PC-S and PR-S. The location of the strain gauges are shown in Figure 4(b)). For the continuous reinforcement case (Figure 16(a)), the middle area ($\pm 500mm$ from the removed column) had the highest strain for loading less than 4.5kN/m^2. However, once cracking started there was a significant change in the stress distribution and yielding occurred across much of the length of the monitored bar. The drops in values can be explained by local variation in stress due to the effect of concrete de-bonding around the steel. Removing the central bottom flexural steel from the

Figure 17: Failure of slab PR-D captured from high speed camera - a) Flexural cracking; b) Shear crack

column location (±400*mm* from the centre) resulted in a different response (see Figure 16(b)). Note that for loading greater than 4.5kN/m^2 the strain gauge at 500mm (gauge S9R) failed and its values have been removed. Due to the non-continuous state of the reinforcement, smaller strain was observed at equivalent loading and positions compared to PC-S, and none of the steel bars yielded. However, an extra gauge (S10R)at -500mm horizontal distance and 450mm away from the edge, is included (marked with o's). This sensor was on the first bar that is continuous along the length and did yield. Strain gauges on the top surface of the concrete, along with visual inspections, revealed that the concrete never underwent crushing.

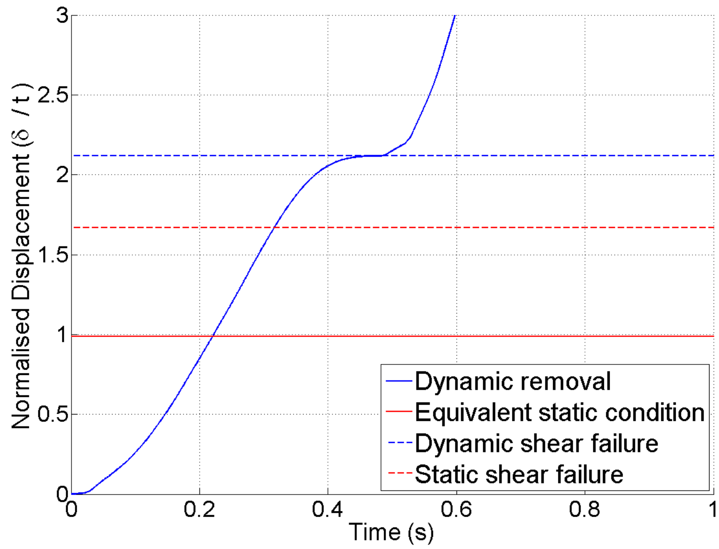

Figure 18: Displacement against time for PR-D at 5.7kN/m^2

4.2.2. *Dynamic removal test*

The failure of the reduced reinforcement condition under dynamic removal with 5.7kN/m^2 of loading is shown in Figure 17, captured by the high speed camera. A wide flexural crack initially occurred due to the lack of tensile reinforcement, before a final shear crack formed leading to complete shear failure, see Figure 17(a) and (b) respectively.

The normalised deflections against slab thickness for this test are plotted in Figure 18, along with the static case at equivalent loading to demonstrate the increase in deflections experienced due to the dynamic effects. In the dynamic case there was a peak displacement of 2.12 times the slab depth, before the shear crack formed at 0.47 seconds. Comparing the results to the static test gives a dynamic displacement amplification ratio of 2.14. However, due to the nonlinear relationship this value is not useful. Extrapolating beyond values from the static force displacement line (Figure 15) gives an equivalent force DAF of only 1.35, based on the assumption that shear failure does not occur. The reduction in stiffness caused by the initial flexural damage might have caused the much higher deflections observed. Furthermore, the maximum vertical reaction at adjacent supports occurred as the slab reaches a temporary static condition at its maximum deflection, this delayed the shear crack forming and allowed higher deflections to be reached. For further comparisons, details of shear failures are given in Table 4.

Considering the strain rate data for the two tests, shown in Figures 19 and 20, demonstrates that moderately high strain rates occurred after the sudden column loss at the higher loadings, in the order of 0.2-0.3s^{-1}. However, as was seen in the corner loss case, the peak strain, and therefore highest stress, in the material occurs after the maximum strain rate. Additionally, at this point, the rate was close to its minimum as the sample was at a temporary rest position between oscillations. Test PC-D in Figure 19 shows that the strain rates in the elastic test are relatively small, around 0.02s^{-1}. Furthermore, most of the monitored points also had small strain rates even at the higher loading. However, strain gauge S3, see Figure 4(b), did show much higher values. This is to be expected from comparing to the static case in Figure 16(a) as that location clearly undergoes yielding. Of further interest is strain gauge S7, which was positioned at the support that was removed. This location quickly switched from a compressive, hogging state, to a sagging, tensile condition, which explains its high strain rate immediately after removal. However, this area became less critical due to further damage occurring across the slab.

Figure 20, showing strain rate data from test PR-D, gives a comparison between maximum strain rates and maximum strain. Additionally, the vertical line

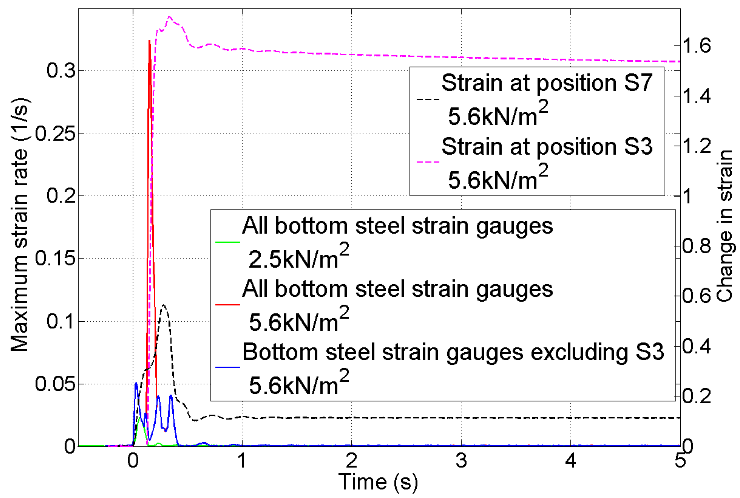

Figure 19: Maximum steel strain rates against time. Also showing changes in strain against time. - Test PC-D

indicates the time at which the shear crack formed. Considering strain positions S3 and S7, it can be seen that the sample had reached its maximum defection and strain and was about to continue its oscillation when the slab failed due to shear. At this time the strain rates were very low at all points across the slab.

The flexural cracks on the underside of the test specimens are shown in Figure 21, Permanent supports (solid boxes) and the removed support (outline) are shown. In both cases there were primary cracks spreading perpendicular to the new support arrangement. The position of the bottom reinforcement mesh is also indicated to show that the orthogonal cracks in the middle area follow the steel positions. This is especially pronounced in PC-D, where the diagonal cracks reach right to the centre line. Whereas for the reduced case (PR-D) it is shown in Figure 21(b) that the cracks were non-continuous at the column loss location and prop-

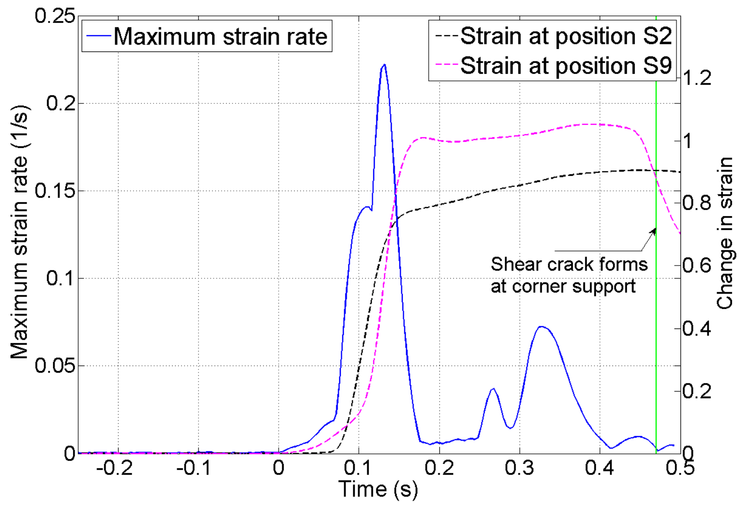

Figure 20: Maximum strain rates against time at 5.7kN/m^2. Also showing changes in strain against time - Test PR-D

agated around the edge of column area, following the reinforcement lines, rather than exploiting the lack of tensile reinforcement in the central area (c.f. Figure 21(a)). However, these cracks were wider and deeper than at other locations and in other tests. For all penultimate removal tests, there was only minimal hogging cracking on the top side running down the centre line, which was followed by shear failures on one or both of the front corner supports (see Table 4).

4.3. *Middle position*

Test M-D was a 4x1 bay continuous slab with a middle column dynamically removed. The change in support reactions from fully supported to the damaged case are shown in Figure 22. Similar to the previous tests, the largest increase in reaction occurred at the supports immediately adjacent to the removal point, whereas the supports further away have a relative reduction in vertical reaction

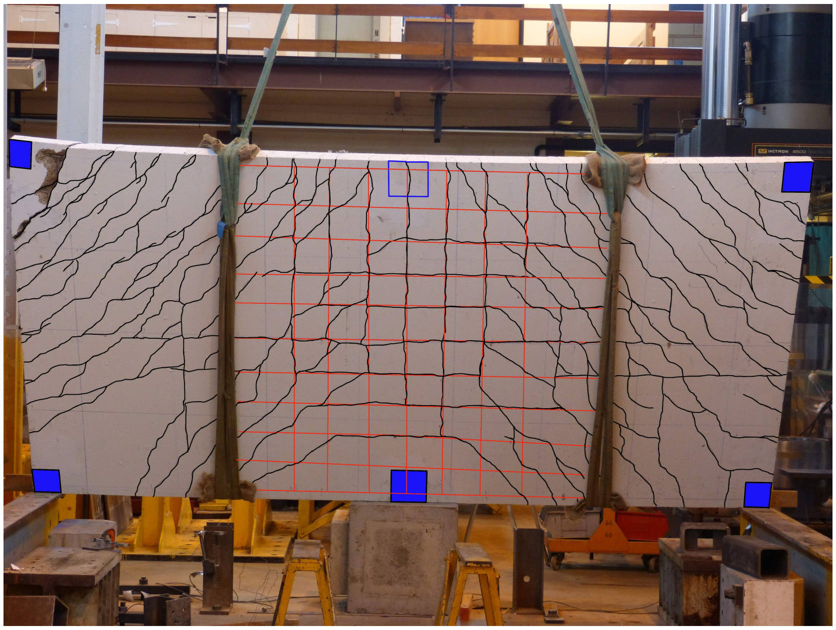

(a) Continuous reinforcement - Test PC-D

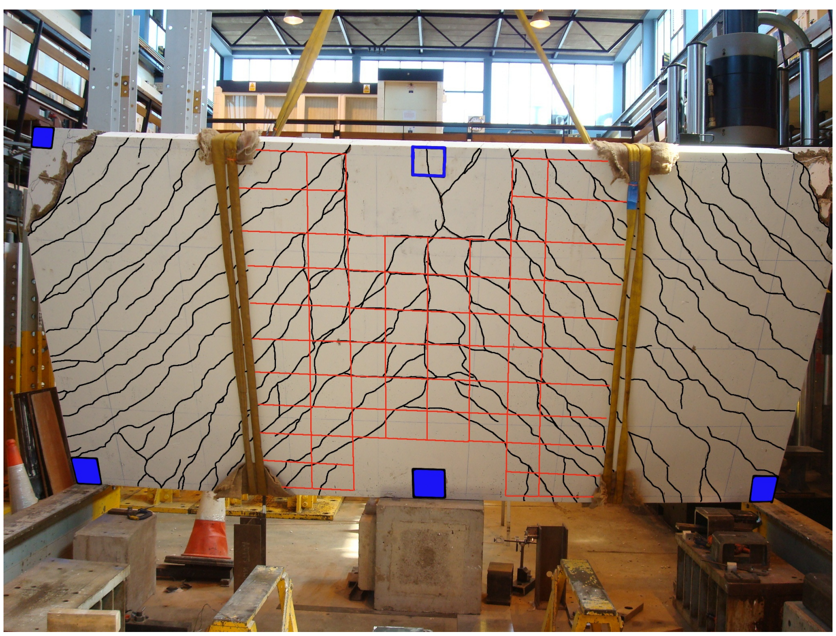

(b) Reduced reinforcement - Test PR-D

Figure 21: Annotated bottom surface flexural cracks and reinforcement after penultimate column loss

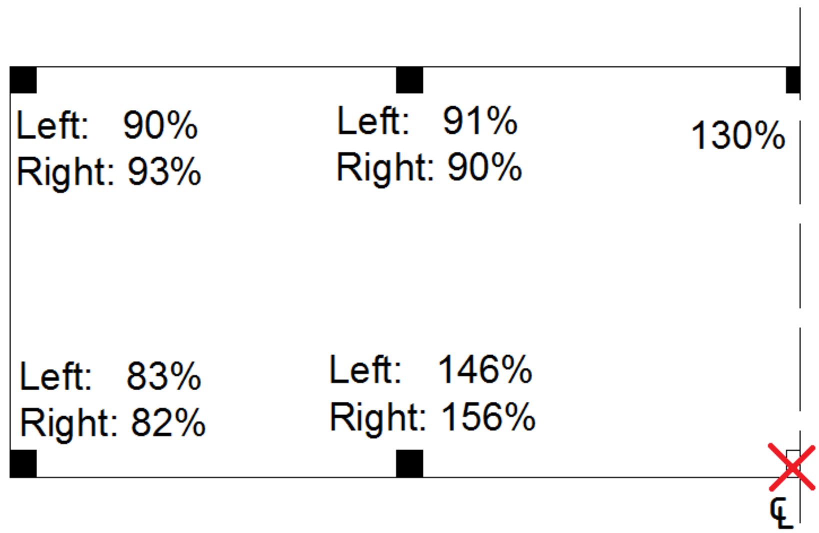

Figure 22: Mean change in distribution of forces to each support after corner column loss - Test M-D

force.

Dynamic removal tests were conducted at different loadings and normalised deflections were calculated using images captured from the high speed camera. Figure 23 compares displacement at the removal location in test M-D for different load levels. Although this arrangement in general shows the same behaviour as the previous tests, there was a significant reduction in the normalised displacements. Comparing the key results given in Table 5 with the equivalent loading for the corner removal case (Table 3), gives a reduction of 55% for the peak displacement in elastic cases. Additionally, at the next loading level (6.8/6.9kN/m^2), the continuous slab peak displacement was only 0.09 times the slab depth, compared to 0.59 in test C-D. As this set up caused a stiffer structure compared to the corner removal tests, displacements are expected to be smaller. Furthermore this also

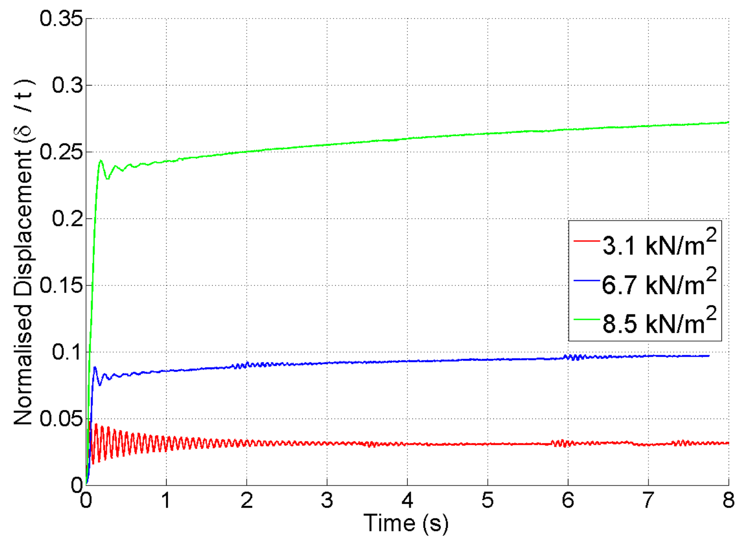

Figure 23: Displacements against time at the removal location for different loadings - Test M-D

meant that the damage, and therefore reduction in stiffness, occurred at a higher level of loading for this case.

At lower levels of load, the bays adjacent to the damaged area experienced a slight uplift, as shown by the negative displacements in Figure 24, due to the slab rotating inwards towards the removed support. Initially, after the column was removed in the 8.5kN/m^2 test, there was a brief uplift (label (A) in Figure 24), however, the damage sustained across the slab resulted in a final downward motion.

Cracking of both the top and bottom surfaces of the concrete led to large plastic deformations and the drift observed in Figures 23 and 24. However, collapse due to total flexural failure did not seem likely and shear cracks did not form within the levels of loads tested (see Table 4).

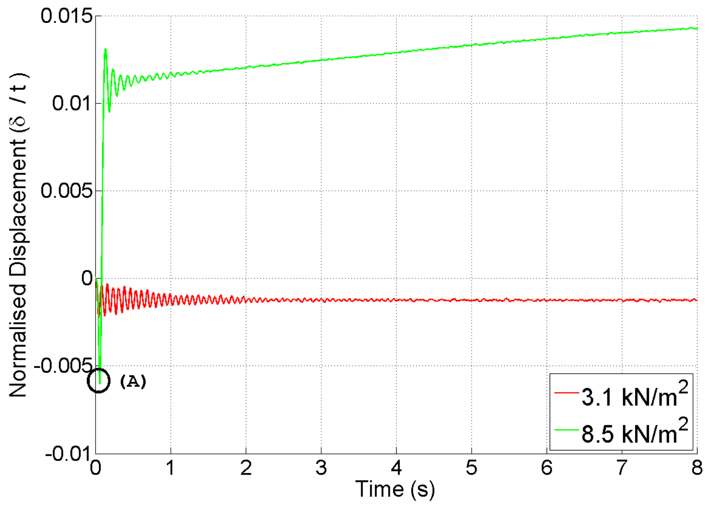

Figure 24: Displacements against time at the center of the adjacent bay for different loadings Test M-D

Based on experimental results, Table 5 gives the values of dynamic effects for three loading levels. In the elastic range (i.e. 3.1kN/m^2) there was a higher natural frequency and a smaller damping ratio. For this the influence of inertial effects on a lightly loaded slab can be seen, resulting in a high peak to final displacement ratio of 1.54. Again increasing the load decreased the frequency of oscillation and increased the damping ratio. For the higher load cases there was an initial dynamic behaviour then, as the major dynamic motion was damped out, the slab underwent further downward deflections under its own self-weight. These displacements became larger than the initial dynamic peak and resulted in further deflections as the slab returned to a static condition. This caused the peak to final displacement ratios of less than 1 presented in Table 5. This behaviour was a result of the damage, and therefore reduction in stiffness, sustained during the

Table 5: Results from dynamic removal - Test M-D

Loading (kN/m^2)	3.1	6.9	8.5
Normalised Peak	0.05	0.09	0.24
Amplitude / Peak (%)	67.31	15.98	5.82
Peak / Final Displacement	1.54	<0.92	<0.90
Damped Natural Frequency (Hz)	13.4	8.55	6.00
Damping Ratio	0.017	0.219	0.204

dynamic response. However, after the period of recording the slab came to rest and complete failure did not occur.

Figure 25 shows a photograph of the underside of slab M-D after the test was completed with the cracks annotated. The primary cracking pattern is shown in black. In this specimen the two-way spanning nature of a slab structure after a column loss is clear by the diagonal cracks. The red lines are secondary flexural cracks that follow the reinforcement lines. As the slab was not continuous in both directions these cracks were more extensive than would be expected in a typical structure. The top cracking due to the increased hogging moments over the adjacent supports was almost identical to the corner removal case shown previously in Figure 7. These cracks followed the same pattern as seen in Figure 21, though were less extensive due to the smaller deflections and the influence of adjacent bays.

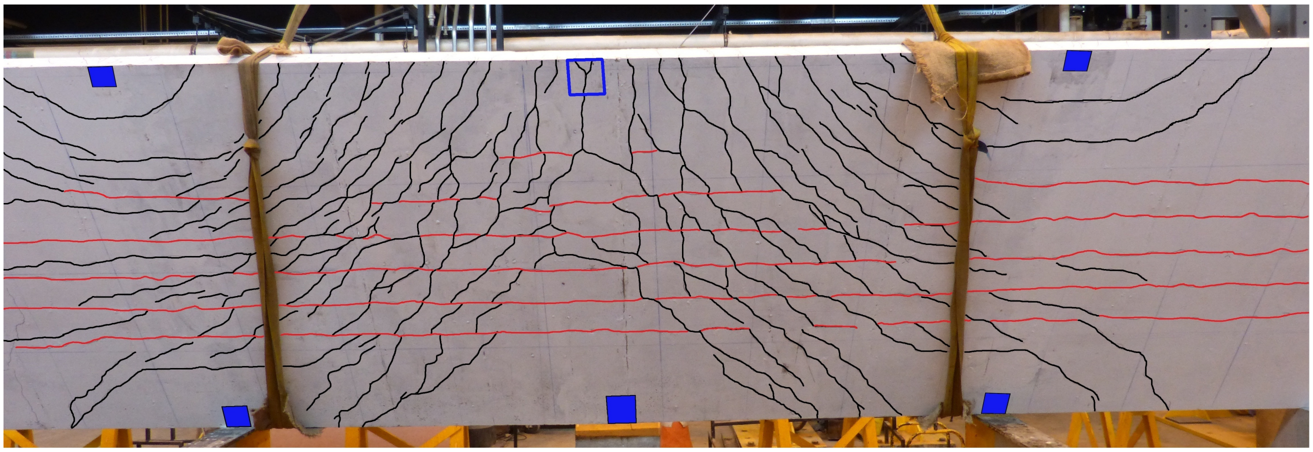

Figure 25: Annotated underside cracking pattern for continuous slab Test M-D

5. Discussion

These tests sought to simulate the effect of a column loss on a flat slab system. The measured reactions forces indicate that each slab was balanced suitably at the start of each test and that the loading was applied evenly across its surface. Analysis of the high speed footage shows that the support was typically completely removed within 50ms. Although this is slower than a true instantaneous column loss scenario caused by an explosion [3, 37], similar removal rates were achieved for all tests allowing comparisons to be made. Furthermore the results still demonstrate the effects of a quick removal. A quicker removal scenario may increase the dynamic effects slightly and will be considered in later numerical analysis.

5.1. Force redistribution

The reaction force distribution and the cracking patterns shown in Figures 6, 7, 14, 21, 22 and 25 give a good indication of the change in load paths that a damaged slab experiences. The test observations indicate that the bending profile becomes truly two-dimensional, with new spans primarily acting diagonally between the nearest supports. The change in spanning arrangement means that the supports closest to the removal location take up the loads that were previously taken from the lost support and a higher proportion of the load on the alternate bay, as shown by the decrease in forces at the further locations in Figures 6 and 22. This increase, potentially more than 50%, might therefore exceed the shear capacity of the slab and lead to a catastrophic failure. Furthermore, simple techniques for analysing moment distributions for flat slabs, such as the equivalent frame method, can not be applied after a column loss.

Increased loading, leading to further damage, does change the distribution of forces slightly due to large rotations, changes in effective span lengths and a local reduction in stiffness after cracking. However, with continuous slabs and restraint provided by columns, these effects will be less significant and so static conditions with small loading may provide suitable information to predict the final demand on the supports.

5.2. Whole slab behaviour

The damage profiles, and results from the two penultimate cases, suggest that the inclusion of continuous reinforcement through a column location does change the distribution of stresses around the removed location. However, there is not a significant difference in ultimate capacity. This is due to the change in load paths away from the removed column. The static tests show that even after cracking has occurred in the concrete and the reinforcement has yielded, the structure can maintain its integrity and show a ductile behaviour. This is partly due to the strain hardening in the steel reinforcement along with geometric nonlinearity as the slab forms a tensile membrane at higher deflections, typically when the peak displacement exceeds half the slab depth. However, the tests emphasised that brittle mechanisms need to be avoided. A particular weakness of flat slab systems appears to be shear failure at corner supports. The additional demand placed on these locations when a neighbouring column is lost, combined with their small shear perimeter, makes them susceptible to progressive failures. Increasing punching shear capacity and ensuring surrounding supports have sufficient ductility can therefore prevent progressive collapse.

Furthermore, although it seems that continuous bottom reinforcement through a column may not be significant for flexural capacity, previous research has demonstrated its efficiency in increasing the post-punching shear capacity of the surrounding supports [23]. Therefore, its inclusion will aid in preventing progressive shear failures.

For a flat slab structure, the global response of the surrounding elements plays a key role as loads are redistributed due to the damage in the slab elements. In these test the adjacent bays acted to counterbalance the damaged area leading to lower deflections. Additionally, the continuous slab condition in tests C-S, C-D and M-D allowed the formation of plastic hinges, which dissipated energy from the system. However, in some cases plastic deformations continued after the test, as shown by peak to final displacement ratios less than 1, which could potentially lead to a later collapse. As the aim of these tests was to investigate the general behaviour of slab elements to validate more detailed numerical modelling, the inclusion of simple supports and non-fixed edges is not considered to be an issue. However, further testing on realistic structural arrangements, including the restraint provided by columns, is required.

5.3. Dynamic effects

The dynamic effects involved in suddenly removing a support can play a significant role in the structural performance of flat slab structures. At low levels of loading, within the elastic limits, there is typically a strong peak in deflections followed by high frequency oscillations until the slab returns to rest after 3 or 4 seconds. At larger levels of loading, the additional mass increases the inertial effect leading to a higher peak and more damage than from a static equivalent. However, the damage also dissipates energy from the system via crack formations and plastic deformations of the steel, resulting in a lower frequency response which is damped out within a second or two. Furthermore, after a sudden removal, forces are not redistributed to surrounding supports instantaneously, with the peak demand occurring as the structure comes to a temporary rest position between oscillations. Therefore, flexural damage may occur before a potential shear failure and create a different response to the static loading case.

Typically in design cases, a factor of 2.0 is applied to the loading in the bays around the removed column during a static analysis to account for dynamic effects. This is based on the behaviour of a linear elastic system with no damping and instantaneous removal and theoretically represents the worst case scenario. However, as all real structures experience some level of damping, it is clear this amplification factor does not reflect a realistic condition. Furthermore, after cracking occurs in the slab there is a reduction in its stiffness creating a nonlinear response. Therefore, at common levels of loading, there is not a direct relationship between the load applied and the level of displacement or damage. This is significant because all observed force factors were considerably less than 2, though further investigations are required to quantify this for typical structures.

The rate of the straining of the steel reinforcement from all the tests indicates that the maximum strain rate is less than 0.35s^{-1}. However, this only occurs at very localised points, which were undergoing significant plastic deformations already, generally the strain rates in the steel were much less than this. High strain rates change the material properties, most significantly increasing the tensile capacity of concrete. To account for this the current Model Code [38], recommends a two phase model, with a higher sensitivity after 10s^{-1}, for calculating the Dynamic Increase Factor (DIF) for concrete due to fast loading.

Using the measured strain rates, the peak DIF the Model Code is 1.26, however, the results demonstrate that at the time of high strains, and therefore stresses, the strain rate is fairly low. This is similar to the results from Yu et al. [39] in their experimental investigation of RC beams under a sudden column loss. They measured strain rates of between 10^{-2} to 10^{-1}/s, and concluded that this only gives a small increase in material strength and can be conservatively ignored. This suggests that the DIF for concrete may not be critical in providing additional flexural capacity.

6. Conclusions

From the above results and discussion, the follow key conclusions can be drawn.

- The sudden column loss idealisation can be reproduced on an experimental substructure of a flat slab floor. The use of a high speed camera with image tracking can monitor deflections for the areas of interest during a dynamic removal condition and capture the formation of cracking. Although true response of a slab structure is dependent on the surrounding elements, a suitable substructure can provide useful information into the key performance parameters.

- The ability of flat slab structures to efficiently span in two directions provides effective alternative load paths after a single column loss. Flexural cracking was observed, both in the sagging areas and hogging over adjacent columns, however, this did not lead to ultimate failure. All observed failures were due to punching shear, usually at corner locations. Progressive shear failures also occurred.

- A reduction in the stiffness of the flat slabs was observed at peak deflections between 0.1 and 0.15 times the slab depth. However, beyond their elastic limit, slab elements can still have significant additional capacity due to material and geometric nonlinearities. As they enter the nonlinear range, there is also a change in the response of the system. Force distributions change and the damage alters the dynamic response of the system. Therefore, to assess the true potential for a progressive failure these effects must be considered.

- The column loss event is inherently dynamic and the level of loading changes the response of the system. This is due to two effects; the increase in mass changes the natural frequency of the system and higher loading results in damage to the structure. When damage occurs the dissipation of energy affects the peak displacement and level of damping, as well as reducing the stiffness, and therefore natural frequency. Additionally, a maximum increase in displacements of 50% more than the static case was observed during elastic tests due to inertial effects. This may therefore cause damage to a structure near its limit, however this effect is less pronounced as the structure experiences permanent damage. Common design recommendations of a load increase of 2.0 appear to be conservative, especially considering the nonlinear relationship between force and displacements after cracking. Furthermore, although high strain rates are known to increase the material strength, the extent of straining and the time profile mean these effects are less significant in assessing the progressive collapse potential.

Acknowledgements

The authors would like to acknowledge the Early Career Research and Knowledge Transfer grant awarded by the University of Nottingham to Dr. Hajirasouliha that funded the project.

References

[1] C. Pearson, N. Delatte, Ronan point apartment tower collapse and its effect on building codes, Journal of Performance of Constructed Facilities 19 (2005) 172–177.

[2] J. D. Osteraas, Murrah building bombing revisited: A qualitative assessment of blast damage and collapse patterns, Journal of Performance of Constructed Facilities 20 (2006) 330–335.

[3] M. Byfield, S. Paramasivam, Murrah Building Collapse: Reassessment of the Transfer Girder, Journal of Performance of Constructed Facilities 26 (2012) 371–376.

[4] J. G. M. Wood, Pipers Row car park collapse: Identifying risk, Concrete (London) 37 (2003) 3.

[5] T. W. Park, Inspection of collapse cause of Sampoong Department Store, Forensic Science International 217 (2012) 119–126.

[6] EN 1990, BS EN 1990: Eurocode 0 - Basis of structural design, 2002.

[7] W. J. Yi, Q. F. He, Y. Xiao, S. K. Kunnath, Experimental study on progressive collapse-resistant behavior of reinforced concrete frame structures, ACI Structural Journal 105 (2008) 433–439.

[8] S. L. Yap, B. Li, Experimental Investigation of Reinforced Concrete Exterior Beam-Column Subassemblages for Progressive Collapse, ACI Structural Journal 108 (2011) 542–552.

[9] K. Qian, B. Li, Experimental Study of Drop-Panel Effects on Response of Reinforced Concrete Flat Slabs after Loss of Corner Column, ACI Structural Journal 110 (2013) 319–329.

[10] M. Sasani, M. Bazan, S. Sagiroglu, Experimental and analytical progressive collapse evaluation of actual reinforced concrete structure, ACI Structural Journal 104 (2007) 731–739.

[11] M. Sasani, S. Sagiroglu, Progressive collapse resistance of Hotel San Diego, Journal of Structural Engineering-ASCE 134 (2008) 478–488.

[12] M. Sasani, S. Sagiroglu, Gravity Load Redistribution and Progressive Collapse Resistance of 20-Story Reinforced Concrete Structure following Loss of Interior Column, ACI Structural Journal 107 (2010) 636–644.

[13] M. Sasani, A. Kazemi, S. Sagiroglu, S. Forest, Progressive Collapse Resistance of an Actual 11-Story Structure Subjected to Severe Initial Damage, Journal of Structural Engineering-ASCE 137 (2011) 893–902.

[14] K. Qian, B. Li, Slab Effects on Response of Reinforced Concrete Substructures after Loss of Corner Column, ACI Structural Journal 109 (2012) 845–855.

[15] K. Qian, B. Li, Performance of Three-Dimensional Reinforced Concrete Beam-Column Substructures under Loss of a Corner Column Scenario, Journal of Structural Engineering-ASCE 139 (2013) 584–594.

[16] Y. Zheng, D. Robinson, S. Taylor, D. Cleland, A. Shaat, Analysis of compressive membrane action in concrete slabs, Bridge Engineering 161 (2008) 2131.

[17] B. Punton, M. P. Byfield, P. P. Smith, Load Redistribution using Compressive Membrane Action in Reinforced Concrete Buildings, Performance, Protection and Strengthening of Structures under Extreme Loading 82 (2011) 272–277.

[18] P. X. Dat, T. K. Hai, Membrane actions of RC slabs in mitigating progressive collapse of building structures, Engineering Structures 55 (2013) 107–115.

[19] L. Keyvani, M. Sasani, Y. Mirzaei, Compressive membrane action in progressive collapse resistance of RC flat plates, Engineering Structures 59 (2014) 554–564.

[20] Y. C. Loo, H. Guan, Cracking and punching shear failure analysis of RC flat plates, Journal of Structural Engineering-ASCE 123 (1997) 1321–1330.

[21] R. L. Vollum, M. A. Eder, A. Y. Elghazouli, T. Abdel-Fattah, Modelling and experimental assessment of punching shear in flat slabs with shearheads, Engineering Structures 32 (2010) 3911–3924.

[22] J. W. Choi, J. H. J. Kim, Experimental Investigations on Moment Redistribution and Punching Shear of Flat Plates, ACI Structural Journal 109 (2012) 329–337.

[23] Y. Mirzaei, M. Sasani, Progressive collapse resistance of flat slabs: modeling post-punching behavior, Computers and Concrete 12 (2013) 351–375.

[24] N. M. Hawkins, D. Mitchell, Progressive Collapse of Flat-Plate Structures, Journal of the American Concrete Institute 76 (1979) 775–808.

[25] D. Mitchell, W. D. Cook, Preventing Progressive Collapse of Slab Structures, Journal of Structural Engineering-ASCE 110 (1984) 1513–1532.

[26] O. Yagob, K. Galal, N. Naumoski, Progressive collapse of reinforced concrete structures, Structural Engineering and Mechanics 32 (2009) 771–786.

[27] W. Yi, F. Zhang, S. Kunnath, Progressive Collapse Performance of RC Flat Plate Frame Structures, Journal of Structural Engineering 140 (2014).

[28] A. J. Pretlove, M. Ramsden, A. G. Atkins, Dynamic Effects in Progressive Failure of Structures, International Journal of Impact Engineering 11 (1991) 539–546.

[29] H. S. Kim, J. Kim, D. W. An, Development of integrated system for progressive collapse analysis of building structures considering dynamic effects, Advances in Engineering Software 40 (2009) 1–8.

[30] O. A. Mohamed, Progressive collapse of structures: Annotated bibliography and comparison of codes and standards, Journal of Performance of Constructed Facilities 20 (2006) 418–425.

[31] L. Kwasniewski, Nonlinear dynamic simulations of progressive collapse for a multistory building, Engineering Structures 32 (2010) 1223–1235.

[32] Q. Kai, B. Li, Dynamic performance of RC beam-column substructures under the scenario of the loss of a corner column-Experimental results, Engineering Structures 42 (2012) 154–167.

[33] S. Pujol, J. P. Smith-Pardo, A new perspective on the effects of abrupt column removal, Engineering Structures 31 (2009) 869–874.

[34] M. H. Tsai, An analytical methodology for the dynamic amplification factor in progressive collapse evaluation of building structures, Mechanics Research Communications 37 (2010) 61–66.

[35] E. 1992, BS EN 1992: Eurocode 2 - Design of concrete structures - Part 1-1: General rules and rules for buildings, 2004.

[36] 2014. URL: `http://www.imetrum.com/`.

[37] D. Cormie, G. Mays, P. D. Smith, Blast effects on buildings / edited by David Cormie, Geoff Mays and Peter Smith, Thomas Telford, 2009. Includes bibliographical references and index.

[38] Fédération Internationale du Béton, Model code 2010 : final draft, Bulletin / Federation Internationale du Beton ; 65-66, International Federation for

Structural Concrete (fib), 2012. Prepared by fib Special Activity Group 5, New Model Code.

[39] J. Yu, T. Rinder, A. Stolz, K. Tan, W. Riedel, Dynamic Progressive Collapse of an RC Assemblage Induced by Contact Detonation, Journal of Structural Engineering 140 (2014).